The Impact of Wet Soil and Canopy Temperatures on Daytime Boundary-Layer Growth

M. SEGAL, J. R. GARRATT,* G. KALLOS,† AND R. A. PIELKE

Department of Atmospheric Science, Colorado State University, Fort Collins, Colorado

(Manuscript received 29 November 1988, in final form 21 July 1989)

ABSTRACT

The impact of very wet soil and canopy temperatures on the surface sensible heat flux, and on related daytime boundary-layer properties is evaluated. For very wet soils, two winter situations are considered, related to significant changes in soil surface temperature: (1) due to weather perturbations at a given location, and (2) due to the climatological north–south temperature gradient. Analyses and scaling of the various boundary-layer properties, and soil surface fluxes affecting the sensible heat flux, have been made; related evaluations show that changes in the sensible heat flux at a given location by a factor of 2 to 3 due to temperature changes related to weather perturbations is not uncommon. These changes result in significant alterations in the boundary-layer depth; in the atmospheric boundary-layer warming; and in the break-up time of the nocturnal surface temperature inversion. Investigation of the impact of the winter latitudinal temperature gradient on the above characteristics indicated that the relative increase in very wet soil sensible heat flux, due to the climatological reduction in the surface temperature in northern latitudes, moderates to some extent its reduction due to the corresponding decrease in solar radiation. Numerical model simulations confirmed these analytical evaluations.

In addition, the impact of synoptic temperature perturbations during the transition seasons (fall and spring) on canopy sensible heat fluxes, and the related boundary-layer characteristics mentioned above, was evaluated. Analogous features to those found for very wet soil surfaces occurred also for the canopy situations. Likewise, evaluations were also carried out to explore the impact of high midlatitude forested areas on the boundary-layer characteristics during the winter as compared to those during the summer. Similar impacts were found in both seasons, regardless of the substantial difference in the daily total solar radiation.

1. Introduction

Surface sensible and latent heat fluxes (or the Bowen ratio) over saturated or very wet surfaces (bare soil or canopy) are affected considerably by the absolute value of the surface temperature (e.g., Priestley 1959; Priestley and Taylor 1972). For very wet surfaces, under given atmospheric conditions, the surface latent heat flux increases as surface temperature increases. The soil surface temperatures, of course, are highly dependent upon the air temperature (e.g., Mahrer and Segal 1985) because of the rapid turbulent exchange between the air and the surface. Therefore, changes of air temperature as a result of synoptic scale weather perturbations at a given location are anticipated to cause a modification in the magnitude of the daytime surface sensible heat flux. Assuming a midlatitude region, the impact of a synoptic cold front passage, or arctic air penetration during the winter, may be involved with a significant fall in the soil surface temperature below its climatological average value. In contrast, the advection of warm air from low latitudes will produce warming of the soil surface above this average value. A similar impact of background temperature on canopy (surface) temperature is to be expected (e.g., Miller 1981).

During the winter and spring in the midlatitudes (which are emphasized in the present study), grazing/agricultural areas are commonly associated with a reduced vegetative cover. Very wet soils are a common feature as a result of frequent snow melt in higher latitudes or due to rain in lower latitudes. Therefore, very wet soil conditions for a range of different surface temperature regimes are likely to occur in the midlatitudes during the winter and spring. At this time of the year, the daytime climatological soil surface temperature decreases significantly toward higher latitudes; Table 1 gives examples of climatological near-surface air temperatures in North America. Based on the foregoing discussion, it is suggested, therefore, that for very wet ground the *efficiency* of the conversion of the surface net radiation into sensible heat flux is larger in higher ratio), is larger in higher latitudes, even though the magnitude of the sensible heat flux is less.

Similarly, canopies which are not under water stress transpire on clear warm days at a significant fraction of the potential evaporation rate. A significant fall in the canopy temperature will result in stomatal closure,

* Present affiliation: CSIRO Division of Atmospheric Research, Private Bag No. 1, Mordialloc, Victoria, 3195, Australia.

† Present affiliation: Department of Applied Physics, University of Athens 10680, Greece.

Corresponding author address: Dr. Moti Segal, Department of Atmospheric Science, Colorado State University, Fort Collins, CO 80523.

TABLE 1. Climatological minimum shelter temperature for several latitudes in Central North America (from *Climatic Atlas of the United States, 1968*).

	Latitude (°N)					
Month	25	30	35	40	45	50
December	285.2	278.2	272.0	266.5	260.4	254.3
January	284.3	277.6	271.5	264.3	256.5	249.9
February	286.0	279.9	273.8	266.5	258.2	252.1
March	288.8	283.2	277.6	271.5	265.4	259.9
April	291.5	286.5	283.2	278.2	273.8	270.4
May	294.3	291.5	287.6	283.7	280.4	277.6
July	296.9	296.5	294.8	292.1	288.7	285.9

and for a given temperature threshold a cessation of the transpiration results, with a corresponding increase in sensible heat flux.

The magnitude of surface sensible heat fluxes is of considerable importance for various daytime atmospheric boundary-layer (ABL) processes; these include (see later for detail)—(i) the time needed for the break-up of the nocturnal surface inversion during the morning, and (ii) the daytime development of the ABL. Additionally, other lower atmospheric processes, including the development of daytime thermally induced flows along slopes, and the erosion of fronts/air masses, are affected by the surface sensible heat flux characteristics. When extensive areas are affected over long periods by a modification in the surface sensible heat flux, some climatic modification may result.

Model studies (e.g., Sasamori 1970; Carlson and Boland 1978; Zhang and Anthes 1982; Wetzel et al. 1984; and Pan and Mahrt 1987 among others) have evaluated the influence of surface wetness on surface heat fluxes, as well as on the ABL characteristics. However, there has been little attention given to the evaluation of the atmospheric temperature effects on these characteristics. The present study provides a general quantitative evaluation of the impact of the surface temperature of very wet soil and canopy temperature on the surface sensible heat fluxes, as well as on daytime related ABL thermal processes. It is worth noting that extensive bare soil areas, resulting from cultivation, are typical in midlatitudes during the winter. Clear sky and snow-free surfaces are assumed in the evaluations. As implied by the discussion presented above, the evaluations are most pertinent for the winter and its adjacent seasonal transition periods. Formulations and general scaling are provided in section 2 (bare soil) and in section 3 (canopy). Analytical and numerical model evaluations of several surface and ABL characteristics are given in sections 4 and 5.

2. Impact of the temperature of very wet soils on sensible heat fluxes

In this section, the formulation of sensible heat fluxes over very wet soil, as a function of the major forcing factors, is provided. In addition, the scaling of some of these factors, as functions of the background temperature and latitude, is presented. A simplified approach is taken, so it is assumed that in *all cases the atmospheric background potential temperature lapse rate is the same*.

a. General formulation

The surface heat balance equation is given by (using the sign convention that non-radiative fluxes are positive away from the surface, radiative fluxes are positive towards the surface):

$$H_s + \lambda E = R_N - G \tag{1}$$

where

H_s sensible heat flux,
λE latent heat flux (λ = latent heat of vaporization),
R_N surface net radiation,
G soil surface heat flux,

with

$$R_N = R_S + R_i - R_0 \tag{2}$$

where

R_S magnitude of solar radiation absorbed at the surface,
R_i magnitude of the atmosphere long-wave radiative flux incoming at the surface,
R_0 magnitude of the long-wave radiative flux emitted from the surface.

Insight into the contribution of the various processes involved with the surface evaporation over saturated soils can be obtained through the so-called combination formulation (Penman 1948; 1956). Following the approach discussed in Webb (1975), Monteith (1981), and Slatyer and McIlroy (1961), we can write the evaporation as:

$$\lambda E = \frac{s}{s+\gamma}(R_N - G) + \frac{\gamma}{s+\gamma}\frac{\rho\lambda(\delta q_a - \delta q_0)}{r_a}, \tag{3a}$$

so that combining this with Eq. (1) yields

$$H_s = \frac{\gamma}{s+\gamma}(R_N - G) - \frac{\gamma}{s+\gamma}\frac{\rho\lambda(\delta q_a - \delta q_0)}{r_a} \tag{3b}$$

where

s $dq_s(T_S)/dT$, with $q_s(T_S)$ the saturated specific humidity at temperature T_S,
γ c_p/λ is the psychrometric constant, with c_p the specific heat of air at constant pressure,
δq_a specific humidity deficit at the reference level in the air,
δq_0 specific humidity deficit at the surface,
r_a bulk aerodynamic resistance to water vapor

transfer (assumed the same as for heat transfer) between the surface and reference level z,

ρ air density.

In Eq. (3a), the first term on the right-hand side reflects the net available energy contribution to the evaporation, and the second RHS term reflects the contribution to evaporation through aerodynamic effects. Equations (3a, b) will be used in the present study for several evaluations outlined in the next sections. However, for simplified scaling purposes, based on Eq. (1), the sensible heat flux at the surface can be expressed as:

$$H_s = \frac{R_N - G}{1 + (1/\beta)} \tag{4}$$

where $\beta \left(= \frac{H_s}{\lambda E} \right)$ is the Bowen ratio.

b. Bowen ratio (β) evaluations

Theoretical considerations by Priestley (1959) suggested that the Bowen ratio over a saturated surface, based on a linearization of the $q_s(T)$ curve, could be given by

$$\beta = \gamma/s \tag{5}$$

though this equation strictly applies only to the special case of saturated air (e.g., Webb 1975). It is also approximately valid in the case of a saturated laminar sublayer near the surface, and represents an upper limit to the Bowen ratio under saturated surface conditions. Priestley and Taylor (1972) argued that a general solution for unsaturated air could be written in terms of an empirical parameter α, given by

$$\lambda E_p = \alpha \left(\frac{s}{s + \gamma} \right) (R_N - G) \tag{6}$$

where E_p is the potential evaporation appropriate to a saturated surface. This implies, through Eq. (4), that the Bowen ratio (again over a saturated surface) is,

$$\beta = \frac{1 - \alpha[s/(s + \gamma)]}{\alpha[s/(s + \gamma)]} \tag{7}$$

in which α is to be determined from observations. Their study suggested its value to be about 1.26 in conditions of negligible cold or warm air advection, though from later studies the suggested value was found to be inappropriate for large roughness surfaces, e.g., forests (Shuttleworth and Calder 1979). In fact Eq. (6) fails to account for "surface" control on E_p, particularly over time periods greater than one day. Nevertheless, as a broad indicator of the surface temperature dependence of β, the limits set by Eqs. (5) and (7) are quite useful.

In the context of the present study, the evaluation of β, or $\Gamma = (1 + (1/\beta))^{-1}$ as dependent on surface temperature, is of considerable importance. We adopted Eqs. (5) and (7) to compute β and Γ within the surface temperature range 248–303 K (Fig. 1). In the computations for surface temperature lower than 273 K (i.e., freezing), $q_s(T_S)$ was defined with respect to the vapor pressure over ice, while λ was corrected to include the latent heat of freezing. The corresponding range in β using Eq. (5) is 0.27 (higher temperature) to 9, while the corresponding range using Eq. (7) is $\approx$0.00 (high temperature) to 7. The dependence of Γ on T_S indicates that, for a given value of $R_N - G$, the corresponding change in H_s within the assigned range of surface temperatures is $\approx$0.1 to 0.9 of $R_N - G$. Thus, the conversion efficiency of available surface thermal energy into sensible heat flux is significantly larger for very low surface temperatures.

c. Additional evaluations

In this subsection specific evaluations providing a generalization and refinement of the evaluations carried out in subsection 3a–b are given.

1) AERODYNAMIC EFFECTS ON SENSIBLE HEAT FLUX

The Bowen ratio, β, given in Eqs. (5) and (7) is based on the assumption that the soil surface is saturated and either i) the assumption of saturated air (Eq. 5), or ii) on an empirically based form which assumes, through a given α, the existence of average surface roughness and moisture properties in the atmospheric surface layer (Eq. 6). It is therefore desirable to elaborate further on its possible modification when departing from these ideal conditions. For example, combining Eq. (3a) with $\delta q_0 = 0$, with Eq. (6) gives,

$$\alpha = 1 + \left(\frac{\gamma}{s} \right) \frac{\rho \lambda \delta q_a}{(R_N - G) r_a}. \tag{8}$$

The experimental data used by Priestley and Taylor (1972) and others imply that the second term on the RHS of Eq. (8) on average $\approx$0.26. For small to moderate z_0 surfaces, this implies a correlation between $R_N - G$ and δq_a, but where large deviations from these average conditions are found, e.g., in strongly advective conditions or where $r_a \rightarrow 0$ for tall transpiring canopies, α may significantly deviate from the assumed value, implying the reduction in the magnitude of sensible heat fluxes in order to maintain a given potential evaporation rate.

2) VERY WET SOILS

Theoretically, the Bowen ratio provided by Eqs. (5) and (7) is applicable for saturated soils, i.e., Eq. (3), with $\delta q_0 = 0$. Observational and theoretical studies suggest that, for a period that may extend as long as several days following saturation, the daytime evaporation is only somewhat reduced from its value during the saturation period. During this period the daytime evaporation is governed by atmospheric conditions,

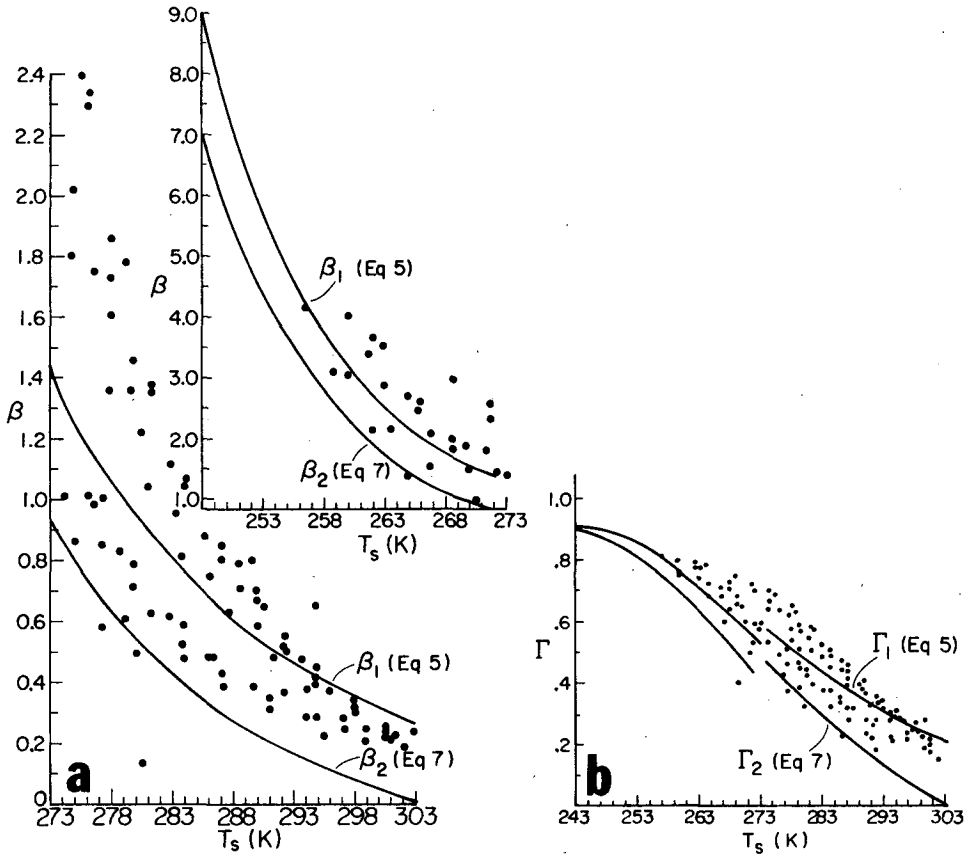

FIG. 1. The dependence of the (a) Bowen ratio, β; and (b) Γ on surface temperature based on Eqs. (5) and (7) (indicated by the labeled solid curves). Dark circles indicate values obtained from the numerical model simulations presented in section 5a.

rather than by soil wetness (e.g., Brutsaert 1982; Hillel 1982). In the following discussion, the impact on the Bowen ratio of departing from the constraint $\delta q_0 = 0$ during this stage is examined.

Adopting Philips's (1957) formulation, the soil surface specific humidity can be approximated as:

$$q(T_s) = q_s(T_s) \exp\left(-\frac{g\Psi}{RT_s}\right) \tag{9}$$

where Ψ is the soil matric potential (i.e., the potential caused by the soil capillary and adsorption forces), T_s is the soil surface temperature, g is the acceleration due to gravity and R is the gas constant for water vapour.

The soil matric potential, Ψ, can be approximated for unsaturated soil (e.g., Campbell 1974; Clapp and Hornberger 1978) as:

$$\Psi = \Psi_s\left(\frac{\eta_s}{\eta}\right)^b \tag{10}$$

where η is the soil moisture content, η_s is soil moisture content at saturation, and b is a constant, which is dependent on the soil type. Adopting values of $\eta_f < \eta < \eta_s$ where η_f is the soil field capacity moisture content (i.e., the level of soil moisture content in which draining and upward water suction are nearly equal), the related values of δq_0 were computed for various types of soils and a temperature range 273–303 K. The computations were carried out using the soil types and physical constants appearing in McCumber and Pielke (1981), and indicated that even when the soil moisture differs significantly from the saturation value, $\delta q_0 \lesssim 1$ g kg^{-1}. Using Eq. (3b) with a typical value of $r_a \approx 100$ s m^{-1} suggests that the increase in H_s due to such a departure from soil saturation (which is considered by the second term in Eq. 3b) is $\lesssim$20 W m^{-2}, accounting in general for less than 25% of the maximum value of the energy term. Thus, it is likely that, for scaling purposes, the conclusions of this study are also valid for very wet, but not saturated, soil.

3. Impact of canopy temperature on the sensible heat fluxes

a. General evaluations

Analogous forms of Eqs. (1)–(3) are used for evaluation of the impact of background temperature on

canopy evapotranspiration λE^c, and consequently on canopy sensible heat flux, H_s^c. Equation (3a) can be used as a reasonable approximation for dense canopy with the constraint $G^c < G$, where G^c reflects thermal losses to the subcanopy layer and the ground, and for a very dense canopy, $G^c \approx 0$. The evaluations provided in section 2 for very wet bare soil are applicable in general for canopy surfaces. However, in the canopy case, stomatal closure and a decrease in the vapor pressure leaf-air difference related to decreases in background temperature should be considered as an additional constraint on λE^c. Using the same arguments applied in the derivation of Eq. (3a), the canopy transpiration can be expressed as:

$$\lambda E^c = \left[\left(\frac{s}{s+\gamma}\right)(R_N - G^c) + \left(\frac{\gamma}{s+\gamma}\right) \times \rho_a \lambda(\delta q_a) \cdot r_a^{-1}\right]\left[1 + \left(\frac{\gamma}{s+\gamma}\right) r_s r_a^{-1}\right]^{-1} \quad (11a)$$

and in analogy to Eq. (3b), by substituting Eq. (11a) into Eq. (1), yields:

$$H_s^c = \left[\left(\frac{\gamma(1 + r_s r_a^{-1})}{s+\gamma}\right)(R_N - G^c) - \left(\frac{\gamma}{s+\gamma}\right) \times \rho_a \lambda(\delta q_a) \cdot r_a^{-1}\right]\left[1 + \left(\frac{\gamma}{s+\gamma}\right) r_s r_a^{-1}\right]^{-1} \quad (11b)$$

where r_s is the bulk stomatal resistance.

Various studies provide the functional dependence of r_s on temperature. Dickinson et al. (1986), for example, adopted a formulation implying a change of r_s between a minimal value at 298 K to an "infinite" value at 273 K. Kaufmann (1984) could not find, in extensive observations in subalpine forested areas located in the Rocky Mountains of Colorado, direct or seasonal effect of temperature on stomatal behavior for temperatures above 273 K. He suggested that above the freezing level, a drop in temperature is involved with a decrease in transpiration of the subalpine forest, merely due to the reduction in the air humidity deficit. However, within the context of the present study, the two approaches suggest a similar effect on transpiration.

In general, for temperatures around 303 K, $r_s \approx r_{s_{0_{min}}}$ (where $r_{s_{0_{min}}}$ indicates the lowest level of stomatal resistance). Based on Eqs. (11a, b), for a transpiring canopy, λE^c and H_s^c are similar in their magnitude to that of very wet soil (λE and H_s; Eqs. 3a, b) under the same environmental conditions. (Assuming $G^c \approx 0$ and considering the energy term, suggests that H_s^c will be somewhat larger than H_s. However, the aerodynamic term in Eq. (11b) is proportional to r_a^{-1} which increases with the surface roughness, thus, reducing H_s^c over a transpiring canopy. Therefore, in general, we expect, as a first approximation, $H_s^c \approx H_s$ for a given available net radiative input). With a decrease in the background temperature, the decrease in λE^c is likely to be larger than the corresponding decrease in λE over very wet bare soil, due to the rapid increase in the bulk stomatal resistance, r_s. When $r_s \to \infty$, and $\lambda E^c \to 0$, then from Eqs. (1) or (11b), $H_s^c \approx R_N - G^c$. Consequently, following a decrease in the temperature below a given threshold, it is likely that $H_s^c > H_s$.

b. Seasonal effect on canopy sensible heat fluxes

During the winter, in the higher midlatitudes, the coniferous canopy transpiration is negligible or absent for the typical environmental background temperature range (since air humidity deficit is reduced, while it is likely that $r_s \to \infty$ for very low temperatures). Obviously, no transpiration occurs with the dormant deciduous trees, and therefore, $r_s \to \infty$ (similarly, native grass areas in low latitudes affected by cold air are characterized by an increased value of r_s). Forested areas in these geographical locations during the winter are, therefore, relatively efficient in the conversion of the available net thermal energy to surface sensible heat fluxes. Obviously, the situation is reversed during the summer except when vegetation is drought stressed. Thus, we suggest that a tendency toward relatively small annual changes in sensible heat fluxes is typical for such locations. Most interesting, however, are the spring and fall periods in which rapid changes in transpiration may occur due to physiological changes in the canopy. Since the absolute day-to-day change in the daily solar radiation amounts during the short transition periods is small, a corresponding rapid change in the canopy sensible heat flux should be observed.

Kaufmann (1984) has evaluated such changes of transpiration patterns for the subalpine Rocky Mountain forest. He computed a decrease in typical daily transpiration values of ~3 mm to a negligible transpiration within ≈2 weeks during the fall (see Fig. 2; ~ week 42). His study also suggests a noticeably sharp increase of daily transpiration within a short period during the spring (see Fig. 2; ~ week 20). These observations imply large resultant changes in the canopy heat fluxes.

c. Synoptic temperature perturbation effect on canopy sensible heat flux

Synoptic weather perturbations are often associated with a large change in the air temperature. Based on the discussion in section 3a, they are likely to cause pronounced fluctuations in transpiration, and consequently, in the sensible heat flux. Such effects are noticeable, for example, in the subalpine Rocky Mountains forest during the spring (weeks 20–24), according to the data adopted from Kaufmann (1984) (see Fig. 2). The sharp changes in the air temperature during that period are reflected in a corresponding change in the daily transpiration rate which should be associated

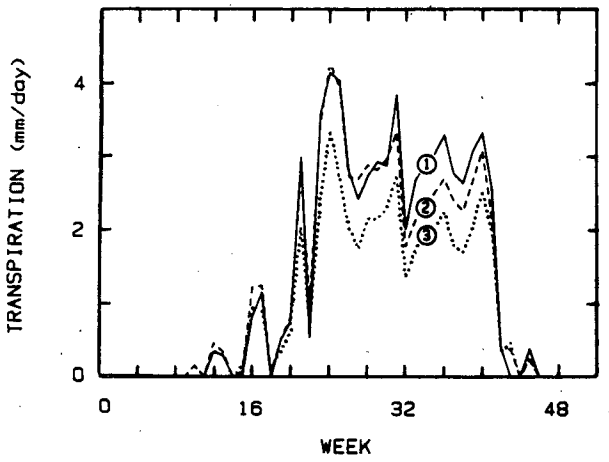

FIG. 2. Annual patterns of daily transpiration amounts at three sites in the Lexen Creek area located in the subalpine forest of the Rocky Mountains, Colorado (week = 0 is the first week of January). Canopy species include: Engelmann Spruce, Subalpine Fir, and Lodgepole Pine (reproduced from Kaufmann 1984).

with a change in the surface sensible heat flux. In lower midlatitudes during the winter, where native grass canopies are typical in areas affected by precipitation, similar patterns are expected due to the occasional penetration of extremely cold air masses to these locations.

4. Boundary-layer analytical evaluations

In section 3, the various factors affecting H_s, as related to a large range of surface and background temperature changes, were evaluated. In the present section, formulations are considered in order to evaluate the related impact on the daytime ABL development.

a. Development of the daytime ABL

Following Tennekes' (1973) and using Eq. (4), the depth of the daytime convective ABL at time t following sunrise, $h(t)$, can be approximated as:

$$h(t) \approx \left[\frac{2\int_0^t H_s d\tau}{\rho c_p(\partial\theta_0/\partial z)} \right]^{1/2}$$

$$= \left[\frac{2\int_0^t \Gamma(T_s)(R_N - G)d\tau}{\rho c_p(\partial\theta_0/\partial z)} \right]^{1/2} \quad (12)$$

where $\partial\theta_0/\partial z$ is the potential temperature lapse rate in the lower atmosphere around sunrise and Γ (as defined in section 2) is dependent on the surface temperature, T_s (a function of time). Equation (12) can be approximated as:

$$h(t) = \left[\frac{2\Gamma(\bar{T}_s)\int_0^t (R_N - G)d\tau}{\rho c_p(\partial\theta_0/\partial z)} \right]^{1/2} \quad (13)$$

where $\Gamma(\bar{T}_s)$ is a representative value of Γ within the specified time period.

The daytime departure of the averaged potential temperature within the atmospheric ABL, $\tilde{\theta}'$, from its sunrise value can be determined from the relation:

$$\tilde{\theta}' \approx \frac{1}{2} h \frac{\partial\theta_0}{\partial z} \quad (14)$$

b. Break-up of the nocturnal inversion during the morning

Adopting Tennekes' (1973) formulation, the time $\mathbf{T}$ needed to erode the nocturnal surface inversion during the morning by the surface sensible heat flux is given by:

$$\mathbf{T} = \left[\frac{2\tau\rho C_p h_0 \Delta_0}{(H_s)_n} \right]^{1/2} \quad (15)$$

where

- τ time scale of the initial increase of sensible heat flux ($\sim 10^4$ sec),
- h_0 initial inversion depth,
- Δ_0 initial surface inversion strength,
- $(H_s)_n$ surface sensible heat flux at noon.

c. Soil surface evaluations

1) THE IMPACT OF A CHANGE IN T_S ON h, $\tilde{\theta}'$, AND $\mathbf{T}$

Assume a given location which is associated with two daily averaged surface temperature values, $(\bar{T}_s)_c$ and $(\bar{T}_s)_w$ [where subscript c denotes cold air, w denotes warm air; $(\bar{T}_s)_w > (\bar{T}_s)_c$], and that the same initial background thermal stability $\partial\theta_0/\partial z$ occurs. Using Eqs. (13) and (14) and defining a parameter $\epsilon_1(t) = h_c(t)/h_w(t) = \tilde{\theta}'_c(t)/\tilde{\theta}'_w(t)$, we have:

$$\epsilon_1(t) = \left[\frac{\Gamma(\bar{T}_s)_c}{\Gamma(\bar{T}_s)_w} \cdot \frac{\int_0^t [(R_N - G)_c]d\tau}{\int_0^t [(R_N - G)_w]d\tau} \right]^{1/2}, \quad (16)$$

which provides an approximation to the relative impact of temperature change on h and $\tilde{\theta}'$. Likewise, using Eq. (15) and defining $\epsilon_2 = \mathbf{T}_c/\mathbf{T}_w$, it readily follows that $\epsilon_2 = \epsilon_1^{-1}$, where ϵ_1 is computed at noon. As discussed in the next section, $(R_N - G)_c$ is likely to be larger than $(R_N - G)_w$ in the stage immediately following the occurrence of cold/warm advection (see Fig. 4). However, after some time $(R_N - G)_c \approx (R_N - G)_w$ as implied by Fig. 5. Therefore, for simplicity, and while considering the above two stages, Eq. (16) can be written as:

$$\epsilon_1(t) \geq \left[\frac{\Gamma(\bar{T}_s)_c}{\Gamma(\bar{T}_s)_w} \right]^{1/2}. \quad (17)$$

Figure 3 provides the values for ϵ_1 for different combinations of $(\bar{T}_s)_c$ and $(\bar{T}_s)_w$ (assuming equality in Eq. 17) where Γ was derived from Fig. 1. For example, in extreme cases when $(\bar{T}_s)_c = 248$ K and $(\bar{T}_s)_w = 298$ K, yields $\epsilon_1 \approx 2$. Thus, the ABL depth for the case $(\bar{T}_s)_c$, will be twice as deep as compared to that corresponding to $(\bar{T}_s)_w$. Similarly, the time for break-up of the same nocturnal inversion strength in $(\bar{T}_s)_w$ will be doubled. Of particular interest is the difference in the daily potential temperature change, $\tilde{\theta}'$, for both cases: assuming $\tilde{\theta}'_w = 1.5$ K, then for $\epsilon_1 \approx 2$, $\tilde{\theta}'_c \approx 3.0$ K. Based on Fig. 3, it is likely that changes in background temperatures resulting in $\epsilon_1 \geq 1.5$, are typical for many geographical locations.

2) THE EFFECT OF A CHANGE IN LATITUDE ON h, $\tilde{\theta}'$, AND $\mathbf{T}$

As indicated previously, the change of the climatological surface temperature, T_ϕ, with latitude (from the midlatitudes poleward) during the winter is large. Thus, the Bowen ratio, as implied by Eqs. (5) and (7), tends to increase poleward; however, the solar radiation, and therefore, $R_N - G$, tend to decrease with increasing latitude.

The impact on the ABL properties h and $\mathbf{T}$ as latitude changes from ϕ_1 to ϕ_2 is given by:

$$\epsilon_3(t) = \left[\frac{\Gamma(\bar{T}_{\phi_1})}{\Gamma(\bar{T}_{\phi_2})} \frac{\int_0^t [(R_N - G)_{\phi_1}] d\tau}{\int_0^t [(R_N - G)_{\phi_2}] d\tau} \right]^{1/2} \quad (18)$$

Thus, using climatological values of $\bar{T}_\phi$ (e.g., Table 1), while being related to measurements or estimations of $R_N - G$, enable the scaling of ϵ_3.

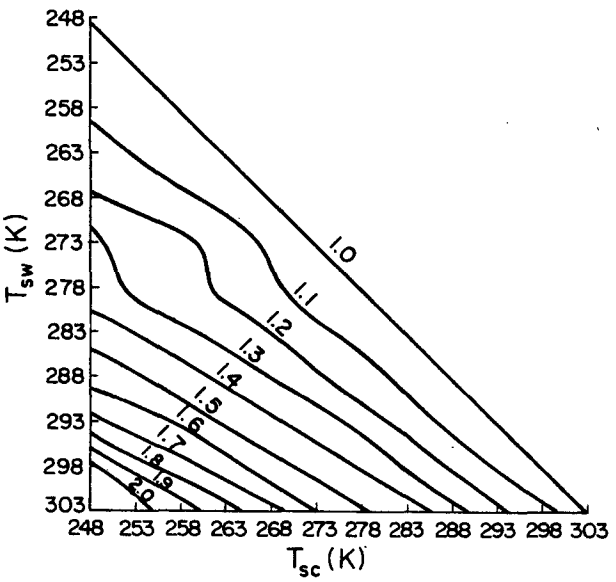

FIG. 3. Values of ϵ_1 as dependent on various combinations of surface temperatures, $(T_s)_c$ and $(T_s)_w$, using Eqs. (7) and (17).

TABLE 2. Input parameters for the numerical model simulations.

Parameter	Value
Surface roughness	
bare soil	0.04 m
vegetation	1.0 m
Soil conductivity	3×10^{-7} m^2 s^{-1}
Initial θ lapse $\left(\frac{\partial \theta_0}{\partial z}\right)$	3.5 K km^{-1}
Initial specific humidity vertical profile	85% relative humidity
Synoptic flow	3 m s^{-1}

Model levels: 5, 10, 20, 30, 40, 50, 75, 100, 200, 300, 400, 500, 600, 700, 800, 900, 1 000, 1200, 1400, 1600, 1800, 2000, 2500, 3000, 3500, 4000, 4500, 5000, 5500, 6000, 7000, 8000, 9000, and 10 000 m.

d. Canopy surface evaluations

As discussed in section 3, the impact of a change in the background temperature on the sensible heat flux is more significant when vegetation is present than for the bare soil case. Therefore, it is probable that the temperature effects evaluated in subsection 4c, for bare soil, are greater in the canopy case. Of most interest, is the seasonal transition periods in which, due to rapid changes in the canopy characteristics, extreme modifications in λE^c and H_s^c may occur over short periods of time, even though solar radiation changes are relatively small.

5. Numerical model evaluations

In order to provide an additional quantification of the evaluations made previously for very wet soil conditions and vegetated surfaces, a numerical model was applied in several illustrative cases in which ABL characteristics are evaluated. In addition, the main forcing terms of the sensible heat fluxes, based on Eqs. (3b) and (11b) and in the relations (12) and (16)–(18) in section 4, are quantified. The model, whose formulation is given in Mahrer and Pielke (1977), and McNider and Pielke (1981), has been validated successfully in various boundary-layer simulations (e.g., Pielke and Mahrer 1975; Segal et al. 1982; Steyn and McKendry 1987, among others).

a. Very wet soils

1) ABL AND SURFACE CHARACTERISTICS AS DEPENDENT ON T_s

The numerical model was used for one-dimensional simulations of mid-December, mid-February, and mid-April solar conditions at latitude 40°N and with the input parameters given in Table 2. Specified initial surface air temperatures, T_s, were at 5 K intervals between 248 and 303 K, where saturated soil conditions were assumed. The simulations commenced at 0600 LST. The initial surface ground temperature was as-

sumed to be the average value of the surface air temperature range stated above (275.5 K). Thus, the selected initial surface air temperature reflects cold or warm air perturbation around an air-soil initial thermal equilibrium at 275.5 K (Case TC). For comparison, a similar set of simulations were carried out where the initial soil surface temperature and the surface air temperature are assumed identical (Case TV). The whole range of initial temperatures considered in the presentation of the results is not necessarily realistic for all the presented months. Therefore, discretion should be applied when selecting a reasonable range of temperatures to be considered for each given month.

Values of the computed β and Γ, based on the numerical model results, are shown in Fig. 1, indicating a general consistency with the theoretical curves for β and Γ based on Eq. (5), at least for $T_s > 278$ K. Below this temperature, simulated values of β and Γ are somewhat higher than those based on the theoretical curve.

Considering the range of surface air temperatures previously stated under the same solar radiation conditions, the related changes of $(R_N - G)$ which are considered in the evaluations of H_s using Eq. 3b, are contributed by $(R_0 - R_i)$ and G. Thus, presenting the model evaluations for the last two variables is useful. The dependence of $(R_0 - R_i)$ on the surface air temperature, T_s, for Case TC is presented in Fig. 4a. When the environment is perturbed by warm air (i.e., initially $T_s > 275.5$ K) the increased value of R_i leads to a

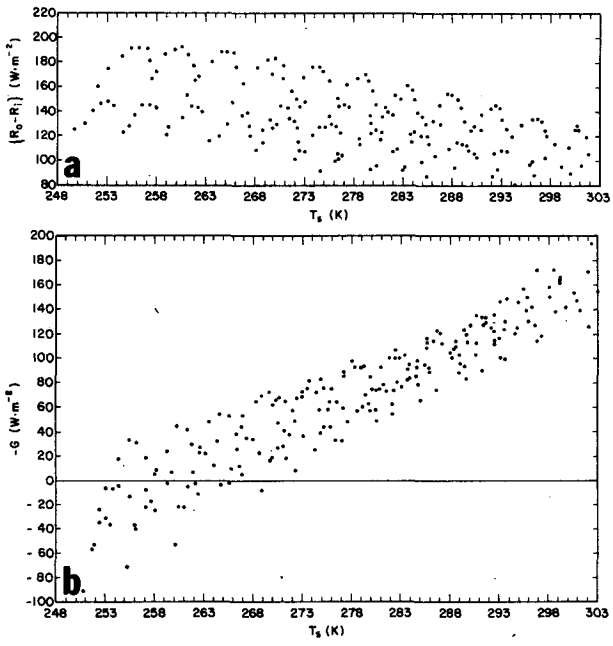

FIG. 4. (a) The dependency of $(R_0 - R_i)$ on the surface air temperature, T_s, based on model simulations for Case TC (saturated soil conditions); and (b) the dependence of G on T_s based on model simulations for Case TC (saturated soil conditions).

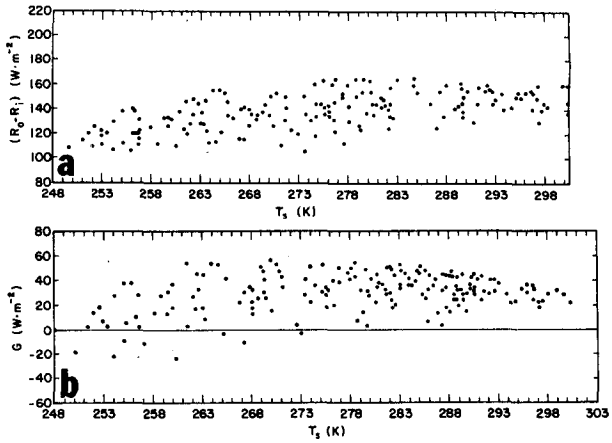

FIG. 5. As in Fig. 4 except for Case TV.

reduction in the magnitude of $(R_0 - R_i)$, while for cold air perturbations ($T_s < 275.5$ K) the reversed situation occurred. However, the difference in the magnitude $(R_0 - R_i)$ between both extreme ranges of temperatures is only $\approx$60 W m^{-2}. A reversed situation is indicated for soil surface fluxes, G; the difference between the extremely low temperature to the extremely high temperature values reached $\approx$200 W m^{-2} (Fig. 4b). It is worth noting that, for the extremely low temperatures, the soil fluxes are toward the surface (i.e., the deep soil provides heat to the surface, contributing to an enhancement of the sensible heat fluxes).

Figure 5a presents the dependency of $(R_0 - R_i)$ on T_s based on the model-computed values for Case TV. The magnitude of $(R_0 - R_i)$ is about constant at the relatively high air temperatures, decreasing somewhat toward the extremely low temperatures. A reversed trend is computed for the soil surface fluxes G (Fig. 5b).

The dependence of $(R_N - G)_a^{1/2}$ and $H_{sa}^{1/2}$ on the initial surface air temperature, T_s, is presented in Figs. 6a–b, where $(R_N - G)_a$ and H_{sa} are the time integrated values of $(R_N - G)$ and H_s, respectively, from the commencement of the simulation at 0600 LST until 1300 LST. With these figures, a quantification relating to the analytical evaluations in section 4 can be made. For the TC cases the $(R_N - G)_a^{1/2}$ values are relatively large for $T_s < 275.5$ K, mostly since a cold air mass over a relatively warm ground suppresses the value of G significantly. On the other hand, for $T_s > 275.5$ K, warmer air over a relatively cooler soil surface enhances the value of G. For the TV cases, the relative change of G and $(R_0 - R_i)$ with a change in T_s is small (see Fig. 5a), consequently, the corresponding change in $(R_N - G)_a^{1/2}$ is relatively small, too. The rate of variation of $(R_N - G)_a^{1/2}$ as a function of T_s, for the TC cases, appears to be nearly the same for the various simulated months. The values of $(R_N - G)_a^{1/2}$ are significantly lower in the mid-winter months primarily due to the reduced solar radiation. For comparison

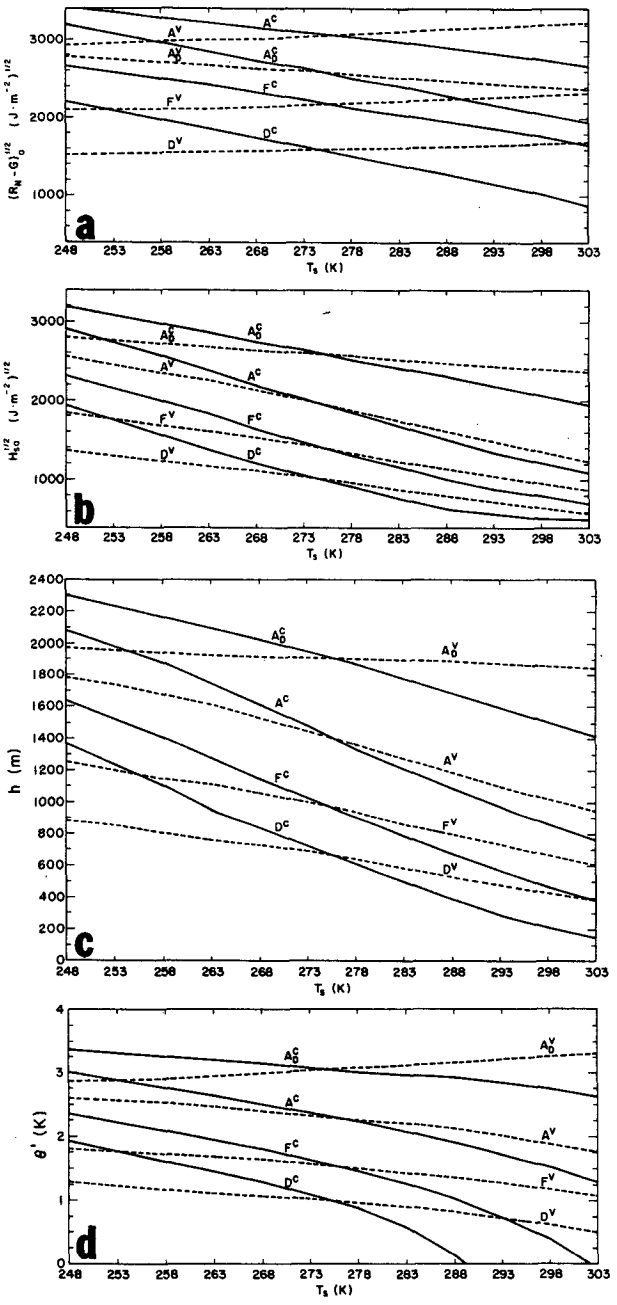

FIG. 6. Simulated time-integrated surface fluxes and ABL characteristics over saturated soil at 1300 LST, as dependent on the initial surface air temperature, T_s, for December (D), February (F), and April (A). The superscripts C and V indicate Case TC and Case TV, respectively, where the subscript D indicates dry soil simulation: (a) $(R_N - G)_a^{1/2}$; (b) $H_{sa}^{1/2}$; (c) the depth of the ABL, h; and (d) the average departure of the potential temperature within the ABL from the initial potential temperature, $\tilde{\theta}'$.

purposes, simulated values of $(R_N - G)_a^{1/2}$ for absolutely dry soil are presented for April (Curves A_D^C and A_D^V). These values are lower when compared with those obtained in the saturated soil case in April (Curves A^C and A^V), since, due to a lack of evaporation from the soil the surface temperatures increase, thus, the magnitude of R_0 and G should also increase.

The values of $H_{sa}^{1/2}$ over the saturated soil are markedly higher or the extreme cold environment for a given month as compared to that of the extreme warm environment (see Fig. 6b). For a reasonable real world range of perturbation in T_s around 275.5 K, the related values of $H_{sa}^{1/2}$ in the simulated cases can vary by about a factor of 1.5 to 2 (Fig. 6b). The impact of saturated soil initial surface air temperature on the magnitude of $H_{sa}^{1/2}$, is illustrated well while comparing it with the corresponding values obtained for the dry soil case (as illustrated for April).

The impact of a variation in T_s on h and $\tilde{\theta}'$ can be evaluated from Figs. 6c–d. It appears to be in agreement with the scaling evaluations given in subsections 4a–c. Changes in these two variables, within a factor of 1.5 to 2, for the indicated range of T_s are likely to be common. It is worth noting that in April for low T_s values the magnitude of those two variables under saturated surface conditions (Curves A^C and A^V) are nearly the same as those obtained in the dry soil conditions simulations (Curves A_D^C and A_D^V).

2) ABL AND SURFACE CHARACTERISTICS AS DEPENDENT ON LATITUDE

The impact of latitudinal change, as reflected in the winter climatological surface air temperature, is simulated with the same initial potential temperature lapse as in the previous simulations. The initial surface air temperatures, T_s, were specified at 5 K intervals between 25° and 50°N as the minimum daily temperature and for the months shown in Table 1. Initially, the soil surface temperature and the surface air temperature are assumed identical (Case TV).

Results are presented for the same variables considered in subsection 5a.1 and using the same model input parameters. The time integrated values of $(R_N - G)$ and R_s at 1300 LST, $(R_N - G)_a$, and R_{sa}, respectively, (Fig. 7a) decrease while moving poleward, most pronouncedly in the midwinter, and primarily due to the reduction in the solar radiation. The related values of $(R_N - G)_a^{1/2}$ and $H_{sa}^{1/2}$ from which ϵ_1, ϵ_2, and ϵ_3 can be determined based on the analysis presented in section 4, are presented in Fig. 7b, c. In contrast to the trends suggested in Fig. 7a, the values of $H_{sa}^{1/2}$ show a general drop only in the high altitudes and in December, January, and February. Of special interest is the slightly higher $H_{sa}^{1/2}$ values for April as compared to May although the $(R_N - G)_a^{1/2}$ values are higher in May. This situation is explained by the higher efficiency of conversion of $(R_N - G)$ into H_s in the relatively lower temperatures in April. Following the spring equinox, a continuous northward increase of $H_{sa}^{1/2}$ values is simulated. The values of h and $\tilde{\theta}'$ (Figs. 7d and 7e, respectively) show the same trends as suggested by

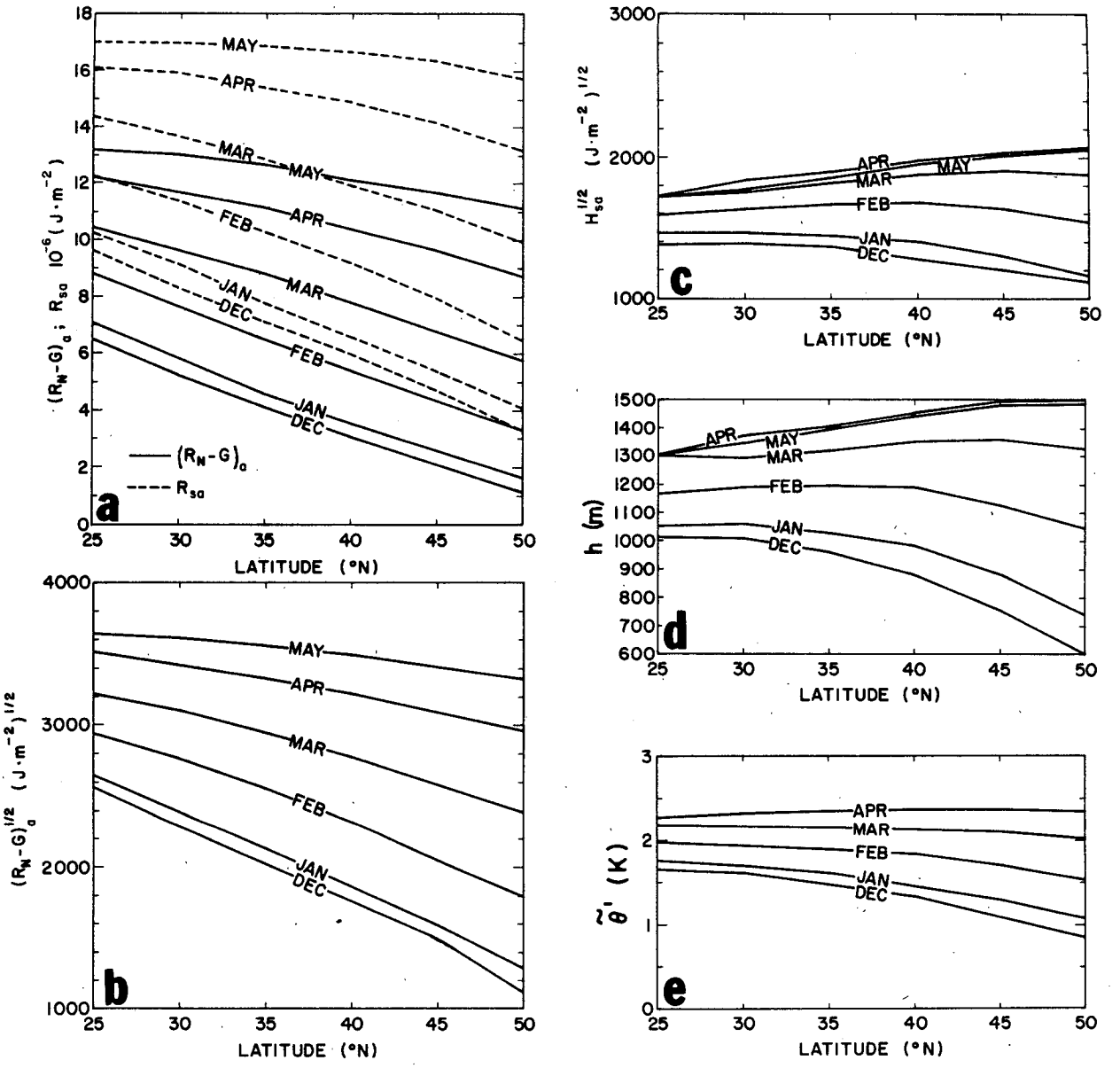

FIG. 7. Simulated time-integrated surface fluxes and ABL characteristics over saturated soil at 1300 LST, as dependent on latitude and month. The initial surface soil temperature is given by Table 1: (a) accumulated $(R_N - G)$ and R_S by 1300 LST; $(R_N - G)_a$ and R_{S_a}, respectively; (b) $(R_N - G)_a^{1/2}$; (c) $H_{sa}^{1/2}$; (d) the depth of the ABL, h; and (e) the average departure of the potential temperature within the ABL from the initial potential temperature, $\tilde{\theta}'$.

the analysis in subsections 4a–c. In the December case, the ratio of $(R_N - G)_a^{1/2}$ at 25°N as compared to its value at 50°N is ~2.3 while the corresponding ratio of h is only 1.7. In April, the corresponding ratio of $(R_N - G)_a^{1/2}$ is ~1.2 where that of h is only ~0.9.

b. *Forested area*

The numerical mesoscale model, which was used in the previous simulations, was also adopted for forest-related evaluations using the vegetation module described in McCumber (1980) and McCumber and Pielke (1981). The simulations deal with two situations: (i) a cessation of transpiration due to stomatal closure in a cold air temperature environment, or when dormant deciduous trees are considered (i.e., $r_s \rightarrow \infty$; which was established by using r_s = 9999 s cm^{-1} in the model simulations); and (ii) substantial transpiration (i.e., full stomatal opening) under relatively high air temperatures (r_s = 1 s cm^{-1}). However, it should be noted that for too high temperatures, coniferous trees experience stomatal control. Therefore, the eval-

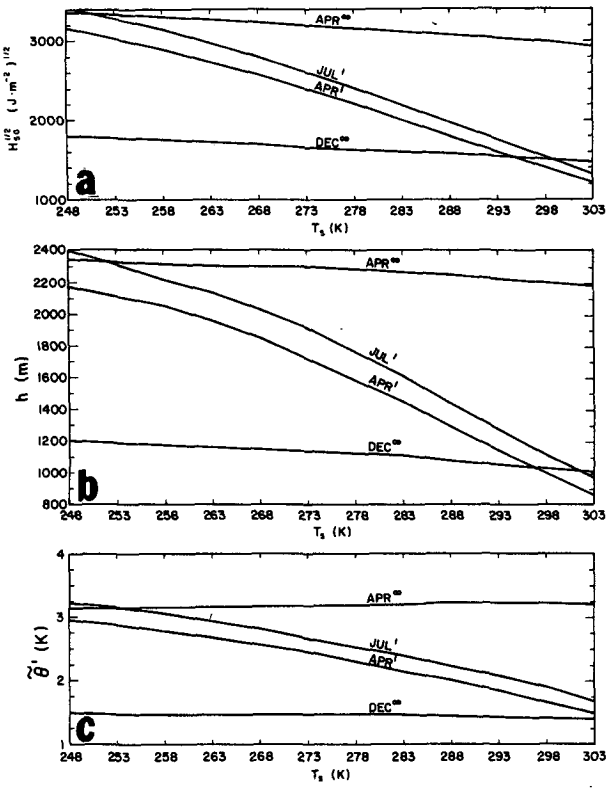

FIG. 8. Simulated sensible heat flux and ABL characteristics over a canopy (Case TV) in December ($r_s \to \infty$), April ($r_s = 1$ s cm^{-1} and $r_s \to \infty$), and July ($r_s = 1$ s cm^{-1}) at 1300 LST and as dependent on the initial surface air temperature, T_s: (a) $H_{sa}^{1/2}$; (b) the depth of the ABL, h; and (c) the average departure of the potential temperature within the ABL from the initial potential temperature, $\tilde{\theta}'$.

uations need to be restricted, in this case, to the temperature range for which significant temperature dependent stomatal control does not occur. Full stomatal opening is likely to occur in the first half of the summer when the soil is wet. In both simulated situations the Case TV was considered. The dependence of $H_{sa}^{1/2}$, h, and $\tilde{\theta}'$ at 1300 LST on the initial surface air temperature, T_s, are presented (Figs. 8a, b, c).

Stomatal closure in December (Curve DEC$^\infty$), due to low temperatures, leads to a slightly increased $H_{sa}^{1/2}$ when the temperature drops, while a somewhat larger corresponding increase is revealed in the April simulation (Curve APR$^\infty$). Corresponding relatively increased values of h and $\tilde{\theta}'$ are simulated. Under a cold air outbreak over a forested area, or native grass area at relatively low latitudes (mostly when the air temperature is $\leqslant$273 K), canopy stomatal closure is anticipated while under moderate warm air advection, close to potential transpiration rate will occur. The difference in April between both situations (while considering, for example, stomatal closure for $T_s < 273$ K and stomatal full transpiration for $T_s > 288$ K) in the value of $H_{sa}^{1/2}$ differs by a factor of $\sim$1.3 to 1.7 (i.e., $\epsilon_1 = \sim 1.3$ to 1.7). The values of $\tilde{\theta}'$ and h are similarly different.

The values of $H_{sa}^{1/2}$ and h in July (JUL^1), assuming the relatively high temperature ranges, are even reduced, compared to those obtained in December (DEC$^\infty$) under low temperatures, and significantly lower as compared to these obtained under low T_s values in April (APR$^\infty$, when stomatal closure is typical).

The simulated results indicate the potential variability in sensible heat flux and ABL properties due to the response of the transpiration to the background temperature. It suggests that on midwinter clear and cold days, a forested area in a higher midlatitude location may generate closely similar sensible heat fluxes, ABL depth and $\tilde{\theta}'$ as compared to those of warm spring days or midsummer days. However, the total solar radiation in the midwinter day may be smaller by a factor of $\sim$2, as compared to that on spring days.

6. Discussion

The present study has evaluated the significance of the level of the background temperature on various properties involved with the ABL over saturated, or very wet, soil surfaces and over canopy surfaces. A scaling approach and numerical model simulations were adopted for this purpose. The relative increase in the efficiency of converting available thermal energy at the surface into sensible heat flux in cold environments as compared with warm environments (where in both environments, the solar radiation is identical) was evaluated based on scaling formulations. It was found that a corresponding increase of several times in the surface sensible heat flux, is not uncommon. Temperature variations, due to horizontal advection at a given location, or due to latitudinal changes, particularly during the winter are considered, with specific relevance to: (i) changes in the depth of the daytime ABL; (ii) changes in the relative daytime warming within the ABL; and (iii) changes in the time needed to break up the nocturnal inversion during the morning. Changes of 50% in (i)–(iii) due to background temperature effects are not uncommon.

Based on the above surface conditions, the study suggests several implications. These suggestions should be considered as an indication of a relative effect (i.e., sensitivity) and not a general result when all the differences (namely, different environmental lapse rates) are included, for example: (i) cold weather conditions provide relatively better vertical dispersion conditions for pollutants (with respect to ABL depth) when compared to conditions with the *same environmental temperature lapse rate,* but which have higher background temperatures; (ii) lower tropospheric convective instability is likely to be enhanced by a significantly reduced environmental temperature for the same temperature lapse rate since the contribution of the surface sensible

heat flux to the lower tropospheric heating will be larger; (iii) modification of the lower atmospheric thermal structure by surface sensible heat flux tends to be more significant in colder environments; (iv) in the high midlatitude locations and under wet soil conditions, forested areas may provide a similar sensible heat flux supply to the atmosphere during winter and the early summer; (v) cold front thermal modification due to surface heating tends to be more noticeable in cold environments; and (vi) in mountainous forested regions, the difference in the sensible heat flux from the canopy in the winter and summer are smaller than is implied by the difference in solar radiation.

Very wet soil conditions occur frequently in midlatitude winter environments as a result of melted snow or rain, with both large nonvegetated and vegetated areas are common in these latitudes. It is suggested that the aforementioned outlined impacts at these latitudes be studied in more detail.

Acknowledgments. This study was supported by the NSF under Grant ATM-8616662 and by EPRI under Contract RP-1630-53. The computations were carried out by the NCAR CRAY computers (NCAR is supported by the NSF). M. Kaufmann provided useful comments while constructive comments by two anonymous reviewers led to the improvement of the manuscript. We would like to thank B. Critchfield and D. McDonald for the preparation of the manuscript.

REFERENCES

Brutsaert, W., 1982: Vertical flux and heat at a bare soil surface. *Land Surface Processes in Atmospheric General Circulation Models,* P. S. Eagleson, Ed., Cambridge University Press, 115–168.

Campbell, C. S., 1974: A simple method for determining unsaturated conductivity from moisture retention data. *Soil Sci.,* **117,** 311–314.

Carlson, T. N., and F. E. Boland, 1978: Analysis of urban-rural canopy using a surface heat flux/temperature model. *J. Appl. Meteor.,* **17,** 998–1013.

Clapp, R., and G. Hornberger, 1978: Empirical equations for some soil hydraulic properties. *Water Resour. Res.,* **14,** 601–604.

Dickinson, R. E., A. Henderson-Sellers, P. J. Kennedy and M. F. Wilson, 1986: Biosphere-atmosphere transfer scheme (BATS) for the NCAR community climate model. NCAR Technical Note 275, 69 pp.

Hillel, D., 1982: *Introduction to Soil Physics.* Academic Press, 364 pp.

Kaufmann, M. R., 1984: A canopy model (RM-CWU) for determining transpiration of subalpine forests. II. Consumptive water use in two watersheds. *Can. J. For. Res.,* **14,** 227–232.

Mahrer, Y., and R. A. Pielke, 1977: A numerical study of air flow over irregular terrain. *Contrib. Atmos. Phys.,* **50,** 98–113.

——, and M. Segal, 1985: Model evaluations of the impact of perturbed weather on soil-related characteristics. *Soil Sci.,* **140,** 368–375.

McCumber, M. C., 1980: A numerical simulation of the influence of heat and moisture fluxes upon mesoscale circulations. Ph.D. dissertation, Department of Environmental Science, University of Virginia, Charlottesville, 255 pp.

——, and R. A. Pielke, 1981: Simulation of the effects of surface fluxes of heat and moisture in mesoscale numerical model. Part I: Soil layer. *J. Geophys. Res.,* **86,** 9929–9938.

McNider, R. T., and R. A. Pielke, 1981: Diurnal boundary-layer development over sloping terrain. *J. Atmos. Sci.,* **38,** 2198–2212.

Miller, D. H., 1981: *Energy at the Surface of the Earth.* Academic Press, 516 pp.

Monteith, J. L., 1981: Evaporation and surface temperature. *Quart. J. Roy. Meteor. Soc.,* **107,** 1–27.

Pan, H-L., and L. Mahrt, 1987: Interaction between soil hydrology and boundary layer development. *Bound.-Layer Meteor.,* **38,** 185–202.

Penman, H. L., 1948: Natural evaporation from open water, bare soil and grass. *Proc. Roy. Soc. London, A,* **193,** 120–145.

——, 1956: Evaporation: An introductory survey. *Neth. J. Agric. Sci.,* **4,** 9–29.

Philip, J., 1957: Evaporation and moisture heat fields in soil. *J. Meteor.,* **14,** 354–366.

Pielke, R. A., and Y. Mahrer, 1975: Technique to represent the heated-planetary boundary layer in mesoscale models with coarse vertical resolution. *J. Atmos. Sci.,* **32,** 2288–2308.

Priestley, C. H. B., 1959: *Turbulent Transfer in the Lower Atmospheric.* University of Chicago Press, 130 pp.

——, and R. J. Taylor, 1972: On the assessment of surface heat flux and evaporation using large-scale parameter. *Mon. Wea. Rev.,* **100,** 81–92.

Sasamori, T., 1970: Numerical study of atmospheric and soil boundary-layers. *J. Atmos. Sci.,* **27,** 1122–1137.

Segal, M., R. T. McNider, R. A. Pielke and D. S. McDougal, 1982: A numerical model simulation of the regional air pollution meteorology of the Greater Chesapeake Bay area—summer day case study. *Atmos. Environ.,* **16,** 1381–1397.

Shuttleworth, W. J., and J. R. Calder, 1979: Has the Priestley–Taylor equation any relevance to forest evaporation? *J. Appl. Meteor.,* **18,** 639–646.

Slatyer, R. O., and I. C. McIlroy, 1961: *Practical Micrometeorology.* CSIRO, 310 pp.

Steyn, D. G., and J. G. McKendry, 1987: Quantitative evaluation of three dimensional mesoscale numerical model of sea breeze in complex terrain. *Mon. Wea. Rev.,* **116,** 1914–1926.

Tennekes, H., 1973: A model for the dynamics of the inversion above a convective boundary-layer. *J. Atmos. Sci.,* **30,** 558–567.

U.S. Dept. of Commerce, 1968: Climatic Atlas of the United States. Environmental Data Service, 80 pp.

Webb, E. K., 1975: Evaporation from catchments. Prediction in Catchment Hydrology, T. G. Chapman and F. X. Dunin, Eds., Aust. Academy of Science. 203–236 pp.

Wetzel, P. J., D. Atlas and R. H. Woodward, 1984: Determination of soil moisture from geosynchronous infrared data: A feasibility study. *J. Climate Appl. Meteor.,* **23,** 375–391.

Zhang, D. L., and R. A. Anthes, 1982: A high resolution model of the planetary boundary-layer—sensitivity test and comparisons with SESAME-79 data. *J. Appl. Meteor.,* **21,** 1594–1609.